

Chapter 2

Modeling and Simulation

C. Brecher, A. Bouabid, M. Deichmueller, B. Denkena, K. Großmann, A. Hardtmann, D. Hömberg, R. Hermes, F. Klocke, M. Löser, O. Rott, P. Steinmann, and M. Weiß

Abstract. One focus of the Priority Program 1180 is the prediction of process machine interactions. The investigated manufacturing processes as well as the machine tool behavior and the physical phenomena vary within the projects of this program. So depending on the issues that were investigated, the modeling approach that is best suitable for the specific problem has to be applied. To predict the interactions these models have to be coupled and simulated. Besides the modeling approaches different simulation techniques have also been applied. This chapter gives an overview of the applied models of the structural machine behavior and the manufacturing processes, the coupling of these models as well as the simulation techniques that were used.

2.1 Introduction

The prediction of process machine interactions requires models of the subsystems “machine” and “process”. Which modeling approach is appropriate for a specific problem depends on the type of process, the character of the investigated interaction and the physical phenomena relevant for this interaction. However, other factors may also have an impact, for example, the computation time or the effort for modeling as well as the effort of a parameter identification based on measured data.

A comprehensive overview of current issues and approaches in the field of predicting process machine interactions is given by Brecher et al. [1]. This chapter focuses on issues that are relevant within the projects of the Priority Program 1180. It gives basic information about the modeling techniques and the coupling methods. Most of the projects within the priority program scrutinized the interactions between the process forces and the static and dynamic displacements at the contact zone of tool and workpiece.

To describe the dynamic behavior of the machine multi-body systems, finite element models and analogous models are applied. The first two approaches contain structural information of the machine. This makes it much easier to apply changes of structural parameters. The analogous models are abstract models where information about the structure is lost but they can be parameterized much easier

using measured frequency response functions. The different approaches to model the machine behavior differ, for example, in terms of degrees of freedom or the ability of coping with nonlinearities.

The applied approaches of process models differ for cutting, grinding and forming processes. In cutting, simple empirical models are applied in most cases. In grinding, empirical models as well as finite element models are applied. In forming simulations, only finite element approaches were used. To couple and simulate the process and machine models coupled simulations as well as model integration within the same software were applied.

2.2 Models of the Machine Behavior

2.2.1 *Multi-Body Models*

A multi-body simulation (MBS) system generally consists of different stiff bodies, which can conduct defined movements. They are connected by different kinds of joints like revolute, prismatic, ball or cardan joints. Movements and reactions of the bodies can be simulated using algebraic-kinematic relations and external forces in the time domain. The main advantage of MBS is the possibility to simulate large scale movements and rotations. In contrary to a MBS a linear FE-simulation e. g. is able to represent the dynamic behaviour of a machine tool only in one defined position. Thus, non-linearities cannot be simulated [2].

In a flexible MBS model, the advantages of both MBS and FE-simulation are combined. As the FEM is able to simulate deformations of parts and the MBS can realize movements of the modelled parts the dynamic machine behaviour can be described for every position of the machine tool slides.

For the implementation of a flexible MBS the structural parts of a machine tool have to be converted into flexible bodies. A flexible body allows the description of its flexible properties in defined points of force transmission. The count of possible part deformations is reduced by means of modal superposition. Hence, linear part deformations can be described by the combination of linear eigenmodes.

Fig. 2.1 shows the difference of a flexible MBS model and a moveable flexible MBS using the example of a machine table. As the flexible MBS uses fixed elements to constrain the machine table to the machine bed the moveable flexible MBS realizes a movement of the machine table. The occurring forces are transferred to the machine bed by dividing the load onto different nodes of the guideway. Hence, a variable load transmission can be realized and the machine behavior can be depicted in more detail.

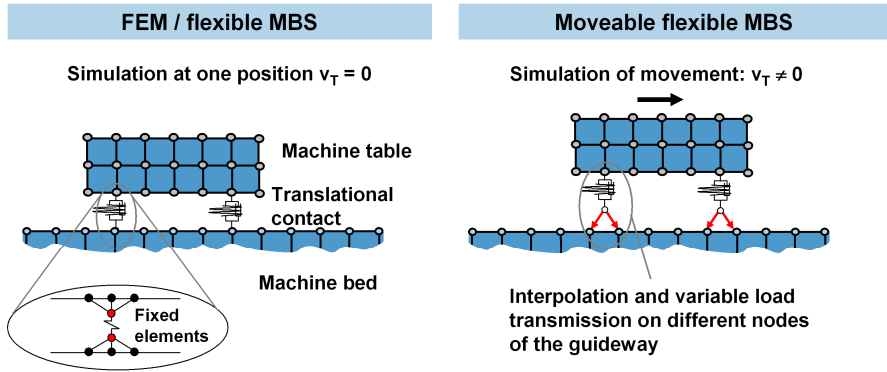


Fig. 2.1 Principle of flexible and moveable flexible multi-body simulation [3]

2.2.2 Finite Element Models

In contradiction to the multi-body systems treated in the last section, structural analyses are primarily concerned with deformable structures, which consist of an infinite number of single material points. Also, structural analyses are more interested in the distribution of physical quantities *within* the structure, e. g. the stress distribution.

In machine tools, the finite element method can be applied in order to analyze both the static and the dynamic machine behavior. In particular, time-dependent and coupled processes are of high interest. Machine tools consist, in many cases, of spinning cylindrical parts, which permit some simplifications of the solution procedure through their form and periodic motion. Then, computationally more efficient solution techniques can be used, e. g. the Arbitrary Lagrangian Eulerian (ALE) approach. In the following, the basics of a transient finite element solution procedure are presented, exemplarily for the case of a spinning wheel, which can represent a grinding wheel, for example. Detailed information can be found in [4]. Bold symbols denote vectors or tensors while scalars are denoted in normal font style.

In the ALE approach, three states (or configurations) of the spinning wheel can be distinguished, Fig. 2.2. B_0 denotes the non-deformed state. In this configuration, each of the material points constituting the wheel can be localized by the coordinates \mathbf{X}_0 . By means of a time-dependent rotation matrix $\mathbf{R}(t)$ one passes to the rotated (or reference) configuration B_r , where material points are described by the coordinates

$$\mathbf{X} = \mathbf{R}(t) \cdot \mathbf{X}_0 \quad (2.1)$$

\mathbf{X}_0 describes the geometry of the spinning wheel at the idle state and does not depend on the time t . \mathbf{X} is time-dependent since the position of a material point changes due to the rotation, regardless of whether the angular velocity ω is constant or not.

Finally, the deformation of the spinning wheel is given at the deformed (or total) configuration B_t by the function φ_0 or φ , depending on the choice of the configuration one takes as reference, i. e. B_0 or B_r respectively. Thus, the coordinates \mathbf{x} of a material point in the total configuration can be given by

$$\mathbf{x} = \varphi_0 (\mathbf{X}_0 , t) = \varphi (\mathbf{X}(t) , t) = \varphi (\mathbf{R}(t) \cdot \mathbf{X}_0 , t) \quad (2.2)$$

The total deformation φ depends on the time t in two ways: indirectly via $\mathbf{X}(t)$ and, in addition, in an explicit way via t . The dependency on $\mathbf{X}(t)$ includes the fact that the less important part of the kinematics, i. e. the rigid body rotation, is anticipated in the model formulation. The direct dependency on time t , however, expresses the most important part of the kinematics, i. e. the transient deformation due to the process forces. For the position vector \mathbf{x} , a total and a partial time derivative $\dot{\mathbf{x}}$ and $\partial_t \mathbf{x}$ can be defined, depending on whether the rigid body rotation is included or not.

$$\mathbf{x} = \varphi_0 (\mathbf{X}_0 , t) = \varphi (\mathbf{X}(t) , t) = \varphi (\mathbf{R}(t) \cdot \mathbf{X}_0 , t)$$

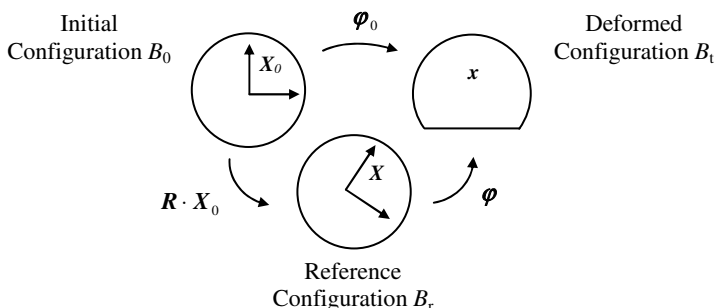


Fig. 2.2 Configurations corresponding to the ALE approach. In addition to the initial non-deformed state and the total deformed state there is an intermediate rotated state one refers to when solving the problem

The stress tensor can be defined in different ways. Relating a force increment $d\mathbf{F}$ to a surface element $d\mathbf{a}$, both in the total configuration, results in the Cauchy or true stress tensor $\boldsymbol{\sigma}$. Taking, however, the surface element in the initial or rotated configuration $d\mathbf{A}_0$ or $d\mathbf{A}$ leads to the Piola-stress tensor \mathbf{P}_0 or \mathbf{P} respectively.

In the following, the basic relations of the finite element model of the spinning wheel are given. All equations are written with respect to the rotated configuration B_r . The balance of momentum writes

$$\text{Div } \mathbf{P} + \mathbf{b}_r = \rho_r \ddot{\mathbf{x}} \quad (2.3)$$

where ρ_r is the material density. The external body forces \mathbf{b}_r , caused by gravity for example, are not important for the present presentation. The total acceleration $\ddot{\mathbf{x}}$

can be determined by totally deriving the position vector \mathbf{x} twice. After some derivations and transformations one obtains the following relations:

$$\text{Total velocity:} \quad \dot{\mathbf{x}} = \mathbf{F} \cdot \dot{\mathbf{X}} + \partial_t \varphi = \mathbf{F} \cdot \dot{\mathbf{X}} + \mathbf{v} \quad (2.4)$$

$$\text{Total acceleration:} \quad \ddot{\mathbf{x}} = \mathbf{G} : \left[\dot{\mathbf{X}} \otimes \dot{\mathbf{X}} \right] + \left[\mathbf{F} \cdot \boldsymbol{\Omega} + 2 \mathbf{L} \right] \cdot \dot{\mathbf{X}} + \mathbf{a} \quad (2.5)$$

Herein, the following entities have been used:

$$\text{Deformation gradient:} \quad \mathbf{F} = \partial_X \varphi \quad (2.6)$$

$$\text{Velocity gradient:} \quad \mathbf{L} = \partial_{X_i}^2 \varphi = \partial_X \mathbf{v} \quad (2.7)$$

$$\text{Gradient of the deformation gradient:} \quad \mathbf{G} = \partial_X \mathbf{F} \quad (2.8)$$

$$\text{Local velocity:} \quad \mathbf{v} = \partial_t \varphi \quad (2.9)$$

$$\text{Local acceleration:} \quad \mathbf{a} = \partial_{tt}^2 \varphi = \partial_t \mathbf{v} \quad (2.10)$$

$$\text{Spin tensor:} \quad [\boldsymbol{\Omega}]_{ij} = \begin{bmatrix} 0 & -\omega \\ \omega & 0 \end{bmatrix} \quad (2.11)$$

$$\text{Guiding velocity:} \quad \dot{\mathbf{X}} = \boldsymbol{\Omega} \cdot \mathbf{X} \quad (2.12)$$

Stresses are related to the strains by means of a material law, e. g. according to the Neo-Hookean model. In this model, the isotropic strain energy function W is given by

$$W = \frac{\mu}{2} \left[\mathbf{C} : \mathbf{1} - 2 \right] - \mu \ln J + \frac{\lambda}{2} \ln^2 J \quad (2.13)$$

The Piola-stress results from the relation

$$\mathbf{P} = \mathbf{F} \cdot \mathbf{S} \quad (2.14)$$

with the Piola-Kirchhoff stress

$$\mathbf{S} = 2 \frac{\partial W}{\partial \mathbf{C}} = \frac{\lambda}{2} \left[J^2 - 1 \right] \mathbf{C}^{-1} + \mu \left[\mathbf{1} - \mathbf{C}^{-1} \right] \quad (2.15)$$

In Eq. (2.13)-(2.15), λ and μ designate the Lamé parameters. In addition, the following entities have been used:

$$\text{Right Cauchy-Green strain tensor:} \quad \mathbf{C} = \mathbf{F}^t \cdot \mathbf{F} \quad (2.16)$$

$$\text{Jacobian of the deformation gradient } \mathbf{F}: \quad J = \text{Det } \mathbf{F} \quad (2.17)$$

Finally, the material stiffness results from

$$\mathbf{C} = 2 \frac{\partial \mathbf{S}}{\partial \mathbf{C}} = 4 \frac{\partial^2 W}{\partial \mathbf{C} \otimes \partial \mathbf{C}} \quad (2.18)$$

Now, when the spinning wheel problem is discretized first with respect to space and then time and when substituting Eq. (2.3) for Eq. (2.4)-(2.12), one can show, that the forces at an arbitrary node I can be written at time step t_{n+1} as:

$$\text{Spinning forces: } \mathbf{F}_{I n+1}^{spn} = - \int_{B_r} \rho_r \left[\partial_X N^I \cdot \dot{\mathbf{X}}^h \right] \left[\mathbf{F}_{n+1}^h \cdot \dot{\mathbf{X}}^h \right] dV_r \quad (2.19)$$

$$\text{Internal forces: } \mathbf{F}_{I n+1}^{int} = \int_{B_r} \left[\mathbf{F}_{n+1}^h \cdot \mathbf{S}_{n+1}^h \right] \cdot \partial_X N^I dV_r \quad (2.20)$$

$$\text{Inertia forces: } \mathbf{F}_{I n+1}^{ine} = \int_{B_r} \rho_r N^I \mathbf{a}_{n+1}^h dV_r \quad (2.21)$$

$$\text{Coriolis-type forces: } \mathbf{F}_{I n+1}^{cor} = \int_{B_r} 2 \rho_r N^I \mathbf{L}_{n+1}^h \cdot \dot{\mathbf{X}}^h dV_r \quad (2.22)$$

where the notation $(\cdot)^h$ means that after spatial discretization the corresponding entity (\cdot) has, of course, to be written in discretized form, i. e. as a function of the value at node I , weighted by the element shape function N^I . The local velocity and acceleration at time step t_{n+1} can be written according to the Newmark-scheme as

$$\mathbf{v}_{n+1} = \partial_t \mathbf{d}_{n+1} \approx \frac{\gamma}{\beta \Delta t} [\mathbf{d}_{n+1} - \mathbf{d}_n] + \left[1 - \frac{\gamma}{\beta} \right] \mathbf{v}_n + \left[\Delta t - \frac{\gamma}{2\beta} \Delta t \right] \mathbf{a}_n \quad (2.23)$$

$$\mathbf{a}_{n+1} = \partial_{tt}^2 \mathbf{d}_{n+1} \approx \frac{1}{\beta \Delta t^2} [\mathbf{d}_{n+1} - \mathbf{d}_n] - \frac{1}{\beta \Delta t} \mathbf{v}_n - \left[\frac{1}{2\beta} - 1 \right] \mathbf{a}_n \quad (2.24)$$

Herein, Δt and \mathbf{d}_{n+1} denote the time increment to be appropriately chosen and the time-dependent nodal position vector to be solved for respectively. Also, it has been assumed that the state of the wheel is known at time step t_n . The parameters β and γ appearing in Eq. (2.23)-(2.24) are the Newmark parameters to be chosen such that

$$(\beta, \gamma) = \left(\frac{1}{4}, \frac{1}{2} \right) \quad (2.25)$$

Relations (2.19)-(2.22) in sum give the force residual vector

$$-\mathbf{R}_{n+1} = \mathbf{F}_{n+1}^{spn} + \mathbf{F}_{n+1}^{int} + \mathbf{F}_{n+1}^{ine} + \mathbf{F}_{n+1}^{cor} \quad (2.26)$$

to be iteratively solved, e. g. by means of the Newton-Raphson procedure when appropriate boundary conditions have been defined. The linearization of the force residual vector \mathbf{R} leads to the stiffness matrix \mathbf{K} , which relates the force at a node I with the displacement at a node J caused by that force. In analogy to the force, the stiffness can be given in form of the following single contributions:

$$\text{Spinning part: } \mathbf{K}_{IJ\ n+1}^{spn} = - \int_{B_r} \rho_r \left[\partial_x N^I \cdot \dot{\mathbf{X}}^h \right] \left[\partial_x N^J \cdot \dot{\mathbf{X}}^h \right] \mathbf{I} dV_r \quad (2.27)$$

$$\text{Geometric part: } \mathbf{K}_{IJ\ n+1}^{geo} = \int_{B_r} \left[\partial_x N^I \cdot \mathbf{S}_{n+1}^h \cdot \partial_x N^J \right] \mathbf{I} dV_r \quad (2.28)$$

$$\text{Material part: } \mathbf{K}_{IJ\ n+1}^{mat} = \int_{B_r} \mathbf{F}_{n+1}^h \cdot \left[\partial_x N^I \cdot \mathbf{C}_{n+1}^h \cdot \partial_x N^J \right] \cdot \left[\mathbf{F}_{n+1}^h \right]^t dV_r \quad (2.29)$$

$$\text{Inertia part: } \mathbf{K}_{IJ\ n+1}^{ine} = \int_{B_r} \rho_r \left[N^I \frac{1}{\beta \Delta t^2} N^J \right] \mathbf{I} dV_r \quad (2.30)$$

$$\text{Coriolis-type part: } \mathbf{K}_{IJ\ n+1}^{cor} = \int_{B_r} \rho_r \left[N^I \quad 2 \frac{\gamma}{\beta \Delta t} \partial_x N^I \cdot \dot{\mathbf{X}}^h \right] \mathbf{I} dV_r \quad (2.31)$$

Herein, \mathbf{I} denotes the identity matrix. By summing all stiffness parts, the total stiffness results in

$$\mathbf{K}_{n+1} = \mathbf{K}_{n+1}^{spn} + \mathbf{K}_{n+1}^{geo} + \mathbf{K}_{n+1}^{mat} + \mathbf{K}_{n+1}^{ine} + \mathbf{K}_{n+1}^{cor} \quad (2.32)$$

which again results together with the force residual \mathbf{R} in the Newton-Raphson step

$$\mathbf{K}_{n+1} \cdot \Delta \mathbf{d}_{n+1} = \mathbf{R}_{n+1} \quad (2.33)$$

where $\Delta \mathbf{d}_{n+1}$ denotes the iterative increment of the nodal displacement vector. Once the nodal position vector \mathbf{d}_{n+1} is known all other entities, e. g. the stress or the strain tensor, can be determined.

2.2.3 Analogous Models

The multi-body and the FE models are based on the structure of the mechanical system. In some cases, it sufficient to describe the dynamic behaviour by abstract models, for example when only the dynamic behaviour at the tool center point (TCP) is of interest for the desired simulation results.

The dynamic behaviour of the structure is represented by a system of masses and spring/dampers, which act like the machine at observed points. In a simple case, the frequency response function at one point can be written as the sum of the frequency responses of n single degree of freedom mass spring damper systems

$$G(j\omega) = \sum_n \frac{1}{-m_n \omega^2 + j\alpha d_n + c_n} \quad (2.34)$$

with the modal mass m , the damping d and the stiffness c . The parameters of these models can be identified from frequency response functions measured at the real

machine structure. For this, commercial software for a modal analysis or self-written routines can be used. In many cases, the fitting between the dynamic behavior of the real structure and the model is better than the one that can be achieved by structure based models, especially in the case of multi-degree of freedom behavior of the machine, see chapter 1. Since the abstract models contain only a few degrees of freedom the computation time for simulations is much shorter than when structure-based models – like FE or MBS models - are applied.

A disadvantage of the analogous models is the loss of information about the structure of the machine. These abstract models are only valid for a given configuration or state of the machine. Therefore, a change of local parameters or a change of the position of the axes can only be considered by a new set of modal parameters. A structure-based model can help to identify local parameters of the real structure that cannot be measured directly. An analogous model is not appropriate for such a task.

2.3 Process Models

2.3.1 *Cutting Force Models*

In addition to the term describing the dynamic machine tool behavior the cutting process term is needed to resemble the process-machine interaction in a closed loop. The cutting process responds to a change in the cutting geometry with an alteration in process forces. The calculation of process forces regarding the dynamic variation of the depth of cut was the priority of the research in the years 1960-1980 [5]. Cutting forces are not only influenced by a relative motion between the workpiece and cutting tool (inner chip thickness modulation) but also by the ripple left on the workpiece surface (outer chip thickness modulation) at the previous revolution (turning) or by the last cutting edge (milling). Not only the modeling of the milling process demands for a considerable effort but also the determination of the force coefficients is known as an extensive procedure. In addition to modeling the determination of force coefficients, which had been defined by the simulation model, was extensive. Radharamanan summarizes the work on this field of research in detail [6].

A common method to estimate the cutting forces acting in turning and milling processes is the analytical description of the interrelationships at the cutting edge [7, 8]. There are three analytical formulations in literature, which differ in their mathematical depiction and the determination of the characteristic force coefficients, Fig. 2.3. The method of mechanistic description is based on the modeling of so-called shear planes. In this regard, a forming process is adopted in the ablated material. The assumed shear stress influences the amount of the calculated process forces decisively. In this context, for example, the shear plane model by Merchant [9] or the "Slip-line field" model by Fang [10] have to be mentioned.

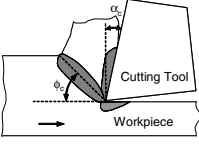
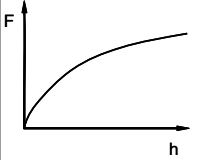
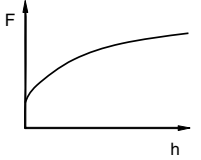
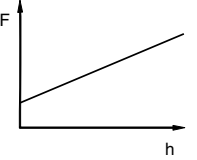
Mechanistic Model	Models based on Exponential Functions		Linear Models
e.g. by Fang et al., Ernst & Merchant $F_s = \tau_s \cdot \left(\frac{b \cdot h}{\sin \phi_c} \right)$ 	e.g. by Kienzle $F_i = b \cdot K_{i1,1} \cdot h^{1-m_i}$ $K_{i1,1} = f(v_c, WZ / WST)$ $1-m_i = f(v_c, WZ / WST)$ 	e.g. by Stéphan, Feng $F_i = b \cdot K_i \cdot h^{x_i} + b \cdot K_{ie}$ $K_i = f(v_c, WZ / WST)$ $x_i = f(v_c, WZ / WST)$ 	e.g. by Altintas $F_i = K_{ic} \cdot b \cdot h + b \cdot K_{ie}$ $K_{ic} = f(v_c, WZ / WST)$ $K_{ie} = f(v_c, WZ / WST)$ 
Model Parameterization through Experimental Analysis	Model Parameterization through Cutting Tests	Model Parameterization through Cutting Tests	Model Parameterization through Cutting Tests

Fig. 2.3 Analytical formulation of cutting forces

Especially for the simulation of process stability linear models and models based on exponential functions have been established to estimate the process forces. Using such simulation models emerging friction between the workpiece and the cutting edge can be captured by appropriate additional terms [7, 11]. These linear models assume a linear relationship between process forces and chip thickness. There are different approaches for this purpose, e. g. by Tlustý [12], Altintas [13] and Weck [14].

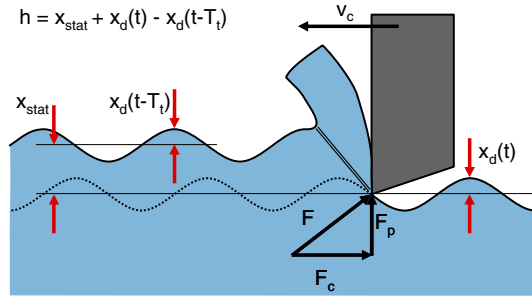
Models based on exponential functions derive process forces out of a non-linear relationship to the chip thickness. Appropriate models for the description of the processes have been developed, for example by Stepan [15] and Feng [16]. Investigations have shown that the feed motion-dependence of the dynamic force variation may explain differences in process stability, which were also partially observed in practice. The parameterization of the shown force models is carried out on the basis of cutting tests and therefore valid only for one defined cutting edge-workpiece material combination. In some cases, the parameterization can be adapted to different experimental conditions with the help of adjusting factors [17].

Especially for the depiction of chip formation, burr formation and the chip temperature the cutting simulation using the finite element method is an important tool [18]. In such a simulation tool, the chip formation is discretized for a small surrounding between the workpiece and the cutting tool by finite elements in a sufficiently small mesh size. These simulations are not linear since large displacements and deformations, temperature and strain rate-dependent plasticity of the workpiece at the cutting point as well as contact between tool and workpiece must be taken into account. The results of the force calculation using FEM do not provide sufficiently accurate results for the passive force in particular.

For mapping the cutting forces in order to simulate the process stability of a machining process in most cases the afore-mentioned analytical models are used. However, the problem is modeling the dynamic cutting forces using data from stationary chipping processes. Fig. 2.4 shows the geometric engagement of a cutting edge for dynamic cutting conditions in one plane. The rapid change of the oscillating engagement conditions leads to digressive results in cutting force calculation.

Regardless of the approach of modeling process forces (mechanistic, empirical) a multiplicity of research works have demonstrated, that dynamic effects have to be taken into account additionally for stability simulation in the case of improving process models. These models consider the inner chip thickness modulation (wave-cutting) and the outer chip thickness modulation (wave-removing) as an independent input parameter as well as a phase shift between the dynamic cutting force and chip thickness modulation.

- The entire current average depth h is composed of static and dynamic portions.
- Location and size of the primary shear zone vary.
- A direct connection between the chip thickness h and the process force F is in contrast to the mechanical conditions .



v_c : Cutting Speed

F : Total Process Force

F_c : Cutting Force (in Direction v_c)

F_p : Passive Force (perpendicular to v_c)

x_{stat} : Static Portion of Tool Deflection

$x_d(t)$: Dynamic Portion of Tool Deflection

$x_d(t-T_t)$: Dynamic Portion of Tool Deflection
Previous Revolution

Fig. 2.4 Plain dynamic cutting

In particular, the variation of the position of the shear plane is quite often used for the determination of the dynamic cutting forces from existing static models. Kim and Lee [19], for example, give an analytical description of the shear angle regarding the inner and outer chip modulation. This dynamic force model considers the transfer function of the tool and its derivation in the direction of cutting speed and direction of the chip thickness variation. Although the mentioned models can be used for stability simulation they have not been applied for this purpose so far.

Van Brussel [20] and Werntze [21] propose simpler, empirical models. These take into account the influence of the inner and outer chip thickness modulation in terms of a proportional relation and a phase shift. The phase shift allows the modeling of a time lag between changes in chip thickness and the corresponding changes in force.

2.3.2 Abrasive Machining

In contrast to conventional machining where workpiece material is removed by a small number of defined cutting edges a large number of abrasive particles or grains acts in abrasive machining processes. In loose abrasive processes like polishing or lapping, the grains are not connected to each other and move independently from each other. In bonded abrasive processes like grinding or honing, the grains are connected by a bond, e. g. resin, vitrified or metal bond. Numerous models to describe grinding processes exist today. They can be divided into fundamental approaches, kinematic models, finite element method (FEM), molecular dynamics, artificial neural networks and rule based models. An overview is given in [22, 23]. Process machine interaction models for grinding are summarized in [1, 24]. Grinding models describe the influence of various parameters like depth of cut or cutting speed on forces, temperatures or surface roughness, for example. Since a universal model for all grinding processes has not yet been developed [25] it depends on the grinding operation and the contact conditions, which model is suitable. In general, the grinding models can be divided into microscopic and macroscopic approaches which are described in the following.

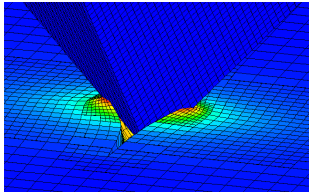
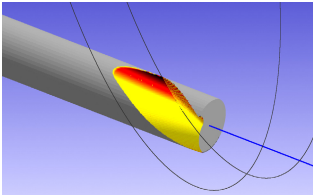
	Microscopic Approaches	Macroscopic Approaches
		
Modelling methods	FEM, Kinematic-geometrical simulations	Kinematic-geometrical simulations (Doxel, Voxel)
Application area	Detailed simulation of chip formation, grinding forces, heat and surface quality	Simulation of material removal, geometric description of contact area, and application of grinding force models
Restrictions	High computation time, high effort to model grinding wheel geometry	Lower resolution in simulation result than with microscopic approaches, surface quality cannot be simulated.

Fig. 2.5 Modeling approaches for grinding processes

2.3.2.1 Microscopic Approaches

The aim of microscopic process models is to calculate e. g. local stresses or temperature, or to gain knowledge on chip formation mechanisms. The microscopic shape of a grinding wheel is determined either by topography measurement [26] or by generative modeling using a mathematical description of the grain morphology [27]. Mostly, statistical methods are applied for modeling the grain distribution [28]. Kinematic-geometrical models, as exemplarily described in [27], assume an ideal chip formation without plowing or similar effects. Process forces are calculated on the basis of undeformed chips of single grains. In other approaches, the finite element method is used to model the engagement of grinding wheel and workpiece [29]. Due to the high computation time, especially of 3D-FEM, only small parts of a grinding wheel are modeled, normally on a small set of grains or single grit scratching tests [30].

2.3.2.2 Macroscopic Approaches

In macroscopic approaches, the grinding process is modeled by calculating the engagement of grinding wheel and workpiece geometrically from a macroscopic view, i. e. no grains are modeled. In macroscopic approaches, parameters like equivalent chip thickness h_{eq} or geometrical contact length l_g are calculated and empirical or FEM grinding force models applied [31]. In the kinematic-geometrical simulation, the workpiece is discretized using dexels, voxels, or boundary representation models, for example. A more detailed description of process models for surface grinding, NC-shape grinding, pendulum and speed stroke grinding and tool grinding can be found in the section “Grinding” of this book.

2.3.3 *Metal Forming*

During an optimal process design the determination of the stresses, forces and energy is an important topic. While the processes of the sheet-metal forming are often limited by workpiece-lateral demands such as tensions and instabilities the process limits of the bulk forming can usually be detected in the tools. Hence, considering temporally and locally different loads the tool and workpiece must be dimensioned in such a way that the tool is predicted from plastic deformations and breakage and the tool wear adjusted to the desired life time. For the optimal machine selection the knowledge of value and localization of the necessary forming force as well as the value of the deformation energy are important. At present, there is a set of methods for the pre-determination of the stresses and forces. Table 2.1 shows a selection of widely-used methods [32].

Table 2.1 Methods for the determination of stresses, forces and energy: d_{xi} - infinitesimal small dimension, k_f – yield stress, V – forming volume, η – deformation efficiency, W – deformation energy, F_m – temporal mean value of deformation force F , σ_c , τ_c – contact stresses, σ_m – temporal and local mean value of normal stress [32]

Increase of simplifying assumptions	Increase of effort and accuracy	Method	Number of d_{xi}	input value	output value
		Method of deformation energy	0	k_f, V, η	σ_m, F_m, W
		Strip method	1	k_f, V, τ_c or μ	$\sigma, F, (W)$
		Slip-line method	2	k_f, τ_c	$\sigma,$
		Method of upper and lower bounds	3	k_f, τ_c or μ	F
		Finite-Element-Method	3	k_f, σ_c, τ_c or μ	σ, F

The methods are tabulated according to the increasing value of an infinitesimal small dimension d_{xi} , which is the basis for the selected section models. Such as the number of simplifying assumptions is reduced, the effort and accuracy of the calculation as well as the number of the included small dimensions are increased. The first two methods are regarded to the elementary theory, the other ones to the higher theory of plasticity.

The majority of elementary methods is valid under the following conditions [33]:

- The workpiece volume remains constant during the forming process.
- The material behaves homogeneously and isotropically, i. e. locally different material properties are generally not considered.
- The elastic deformations are negligibly small compared with the plastic deformations.
- The yield stress is given as function of material, (equivalent) strain, strain rate and temperature.
- The material behavior follows the Tresca’s yield criterion (Maximum Shear Stress Theory) and the *v. Mises*’ yield criterion (Distortion Energy Theory) respectively.
- The contact shear stress is given with a friction formulation, e. g. using the friction value μ or the friction shear factor m .
- Forces of inertia and weight are neglected.

The most frequently applied theoretical methods are

- Method of deformation energy,
- Strip method,
- Slip-line method,
- Method of the upper and lower bounds,
- Method of weighted residuals and
- Finite-Element-Method.

The method of deformation energy is the most elementary method to calculate the deformation forces. This method is based on the law of energy conservation with the applied outer energy

$$W_a = F \cdot s \quad (2.35)$$

equating the inner strain energy

$$W_i = \frac{1}{\eta} k_{fm} V \cdot \varphi. \quad (2.36)$$

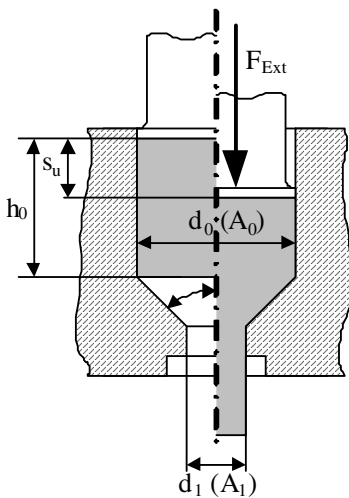
In this formula, k_{fm} is the mean value of yield stress and φ the equivalent plastic strain. The inner energy is equivalent to the total deformation energy

$$W_{tot} = W_{id} + W_{FR} + W_{Sh} + W_B, \quad (2.37)$$

summarizing the expressions for ideal, frictional, shearing and bending energy. The ratio of ideal deformation energy and total deformation energy is referred to as the deformation efficiency

$$\eta = \frac{W_{id}}{W_{tot}}. \quad (2.38)$$

With these preliminary considerations, the determination of deforming forces can be derived for several forming processes. In order to exemplify this procedure the derivation of the forming forces is shown for solid forward extrusion and deep drawing in Fig. 2.6 and Fig. 2.7.



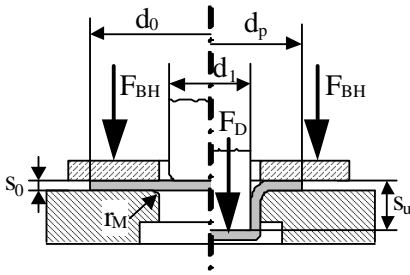
$$W_a = F_{Ext} \cdot s_u, \quad W_i = \frac{1}{\eta} k_{fm} V \cdot \varphi$$

$$\text{with } V = A_0 s_u \text{ and } \varphi = \ln \frac{A_0}{A_1}$$

$$W_a = W_i : F_{Ext} \cdot s_u = \frac{1}{\eta} k_{fm} A_0 s_u \cdot \ln \frac{A_0}{A_1}$$

$$F_{Ext} = \frac{1}{\eta} k_{fm} A_0 \cdot \ln \frac{A_0}{A_1} \quad (2.39)$$

Fig. 2.6 Solid forward extrusion



$$W_a = F_{D,\max} \cdot s_u, \quad W_i = \frac{1}{\eta} k_{fm} V \cdot \varphi$$

$$\text{with } V = \pi d_1 s_0 \cdot s_u \text{ and } \varphi = \ln \frac{d_1}{d_0}$$

$$W_a = W_i :$$

$$F_{D,\max} \cdot s_u = \frac{1}{\eta} k_{fm} \pi d_1 \cdot s_0 \cdot s_u \cdot \ln \frac{d_1}{d_0}$$

$$F_{D,\max} = \frac{1}{\eta} k_{fm} \pi d_1 s_0 \cdot \ln \frac{d_1}{d_0} \quad (2.40)$$

Fig. 2.7 Deep drawing of a cylindrical cup

In both examples, the friction, shear and bending behavior are summarized in the deformation efficiency factor. More detailed approaches considering the friction between die and workpiece result in the following formulas, calculating the maximal forming forces in solid forward extrusion [34]

$$F_{Ext} = k_{fm} A_0 \cdot \left[\frac{2}{3} \tan \alpha + \left(1 + \frac{\mu}{\sin 2\alpha} \right) \ln \frac{A_0}{A_1} \right] + \pi \cdot d_0 \cdot k_{f0} \cdot \mu \cdot h_0 \quad (2.41)$$

and for deep drawing processes [35]

$$F_{D,\max} = \pi d_m s_0 \left[e^{\frac{\mu\pi}{2}} \left(1.15 k_{fml} \cdot \ln \frac{d_p}{d_m} + \frac{2 \cdot \mu F_{BH}}{\pi d_m \cdot s_0} \right) + k_{fml} \frac{s_0}{2r_M} \right]. \quad (2.42)$$

This includes the blankholder force F_{BH} , the mean wall diameter $d_m = d_1 + s_0$ and the outside diameter of the flange when the drawing force has achieved a maximum value $d_p = \sqrt{0.7d_0^2 + 0.3d_m^2}$.

The presented elementary methods provide a solution for a set of problems without substantial effort. This is achieved with simplifying assumptions deviating from the real behavior. If the simplifying assumptions do not meet the requirements of accuracy, the Finite-Element-Method (FEM) could be used, however, with a higher effort and costs. Thus, the following factors can be considered in an improved way:

- different material characteristics,
- complicated geometry of the parts as well as

- inhomogeneous and unsteady mechanical and thermal behavior.
- The FEM is used in metal forming for the simulation of forming processes to determine instantaneous and intermediate states as well as the design of highly-stressed active elements of metal-forming tools (e. g. forging or extrusion dies) [36].

2.4 Coupling of Models

2.4.1 Analytical Considerations

2.4.1.1 General Setting

In general, independent representations for structure and process are the starting point for the development of models describing the process-structure interaction. Depending on the properties of interest engineers can choose among a large variety of structure models. Mathematically, structure models are understood as equations of motion corresponding to

- a complex multi-body system,
- an abstract system with multiple degrees of freedom describing the dynamics of a selected point of a large structure,
- a system of partial differential equations discretized with finite elements in space,
- a coupled system of ordinary and discretized partial differential equations.

The above-mentioned models can be summarized by the following system of differential (algebraic) equations

$$M(t, q, p_M) \ddot{q} = f(t, q, \dot{q}, p_f), \quad (2.43)$$

with p_M, p_f denoting parameter vectors, which are usually determined fitting structure simulation results to the corresponding experimental data. The vector q represents the general set of coordinates. If (2.43) has been directly derived from modal analysis data, the mass matrix is usually constant and the right hand side is a linear function of q and \dot{q} .

Process models relate a geometrical parameter vector g and the relative velocity v between tool and workpiece to the cutting force vector F acting on the tool. In milling, the geometrical parameter vector consists of cutting width b and uncut chip thickness h . A large class of process models can be expressed in terms of the force they exhibit

$$F = \tilde{F}(g, v, p_g), \quad (2.44)$$

where p_g represents an empirical parameter vector depending on tool and workpiece material and on the tool geometry, see section 2.3.1.

In stationary cutting or grinding processes with sufficiently small cutting forces, the geometrical parameters and the relative velocity do not deviate notice-

ably from the desired values regulated by the machine control system. However, if the cutting forces become large, increasing machine structure oscillations induce larger variations of the geometry parameter vector and the relative velocity. This, in turn, leads to undesired cutting force variations, which possibly cause a further increase of the machine structure oscillations. In order to describe these process structure interaction phenomena both aspects have to be incorporated into the model equations. The variation of the geometrical parameter can be formulated as a non-linear functional involving the history of the state variable arising from the structure model (2.43), i. e.

$$g = [t, q(\cdot)] = \int_{t_0}^t \tilde{g}(s, q(s)) ds . \quad (2.45)$$

The relative velocity between tool and workpiece is usually also a non-linear function depending on the state variable and the corresponding time derivative, i. e.

$$v = \tilde{v}(t, q, \dot{q}) \quad (2.46)$$

Moreover, an additional term appearing on the right hand side of (2.43) has to be introduced to model the effect of the varying process forces arising from (2.44) and (2.45), (2.46). Since the forces usually act on the tool or, in terms of the structure model, on an element representing the tool an additional model equation has to be developed to get the appropriate contribution to the right hand side of (2.43). In a general setting, such an expression is given by

$$f_F = \tilde{f}_F(t, q, F) . \quad (2.47)$$

Thus, the modified structure model involving the additional term due to the presence of process forces reads

$$M(t, q, p_M) \ddot{q} = f(t, q, \dot{q}, p_f) + \tilde{f}_F(t, q, F) \quad (2.48)$$

As outlined above, phenomena related to process structure interactions can be modeled by strongly coupled systems, possibly involving the history of the state variable. The equations (2.48), (2.47), (2.46) and (2.45) are an abstract example for the model equation corresponding to an interacting system. In each application, the adoption of the general system may lead to different equations, which have to be solved with tailored numerical algorithms, as shown in the following sections. However, in order to illustrate the different aspects of the general model we focused on a simple milling system at first.

2.4.1.2 Example: A Simple Milling System

A simple system possessing all the important features to model stability problems in milling is illustrated in Fig. 2.8.

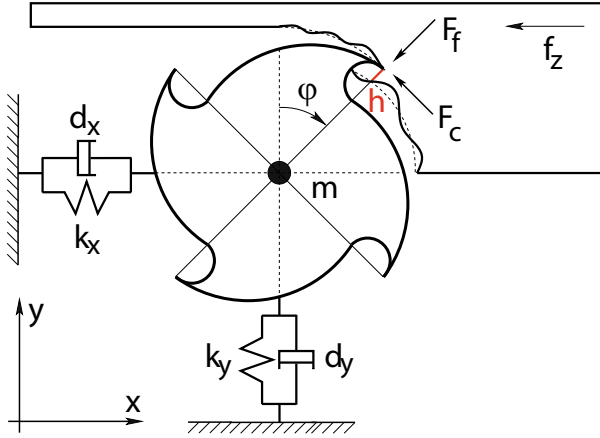


Fig. 2.8 Scheme of a simple milling system

For the present example, the equation of motion representing the machine structure reduces to the system

$$\begin{pmatrix} m & 0 \\ 0 & m \end{pmatrix} \begin{pmatrix} \ddot{x} \\ \ddot{y} \end{pmatrix} = - \begin{pmatrix} d_x & 0 \\ 0 & d_y \end{pmatrix} \begin{pmatrix} \dot{x} \\ \dot{y} \end{pmatrix} - \begin{pmatrix} k_x & 0 \\ 0 & k_y \end{pmatrix} \begin{pmatrix} x \\ y \end{pmatrix} + \begin{pmatrix} F_x \\ F_y \end{pmatrix}, \quad (2.49)$$

The unknown model parameters are $p_M = m$ and $p_f = (d_x, d_y, k_x, k_y)^T$. Note that (2.49) is a very simple form of (2.48). The cutting force model corresponding to (2) is a linear function relating the cutting cross section h a_p and the cutting forces acting on the tip of the cutting edge, i. e.

$$\begin{pmatrix} F_f \\ F_c \end{pmatrix} = \begin{pmatrix} K_f \\ K_c \end{pmatrix} a_p h. \quad (2.50)$$

The parameter vector is $p_g = (K_f, K_c)^T$. The expression corresponding to (2.45), i. e. the variation of the geometrical parameter, consists of a stationary part h_{stat} and a dynamic part h_{dyn} . The dynamic part h_{dyn} represents the modulation of the uncut chip thickness due to the structure oscillations

$$h = h_{stat} + h_{dyn} = f_z \sin \varphi + (x(t) - x(t - \tau)) \sin \varphi + (y(t) - y(t - \tau)) \cos \varphi \quad (2.51)$$

Note that instead of h nonlinear models usually involve the positive part of the uncut chip thickness, i. e. $h_+ = \max(h, 0)$. Since the cutting force components in (2.50) are given in the rotating reference frame of the cutter an additional transformation has to be introduced to get the corresponding force components into the global reference frame, i. e.

$$\begin{pmatrix} F_x \\ F_y \end{pmatrix} = -\gamma(\varphi) \begin{pmatrix} \sin \varphi & \cos \varphi \\ -\cos \varphi & \sin \varphi \end{pmatrix} \begin{pmatrix} F_f \\ F_c \end{pmatrix}, \quad (2.52)$$

with $\gamma [0, 2\pi] \rightarrow \{0,1\}$ denoting a function that switches from one to zero, if the corresponding tooth is not cutting. Again, equation (2.52) can be interpreted as a simple version of (2.47). Since the expressions for the cutting forces, the uncut chip thickness, and the transformation of the cutting forces are given explicitly (2.52), (2.51), (2.50) and (2.49) can be summarized by the following first order delay differential equation (DDE)

$$\dot{u}(t) = [A - C(t)]u(t) + C(t)u(t - \tau) + b_{stat}(t), \quad (2.53)$$

where $C(t)$ denotes a non-smooth τ -periodic matrix. The vector $b_{stat}(t)$ represents the external forces related to the stationary uncut chip thickness h_{stat} . The incorporation of process structure interaction effects leads to an additional state-dependent term h_{dyn} in the uncut chip thickness (2.51). Without this term the matrix $C(t)$ vanishes and (2.53) reduces to an inhomogeneous linear ordinary differential equation (ODE) with constant coefficients. Simulating the solution of (2.53) with the Matlab dde23 solver and comparing it to the corresponding solution $v(t)$ of the system with $C(t) = 0$ for two different values of a_p reveals the additional benefit of the interaction model.

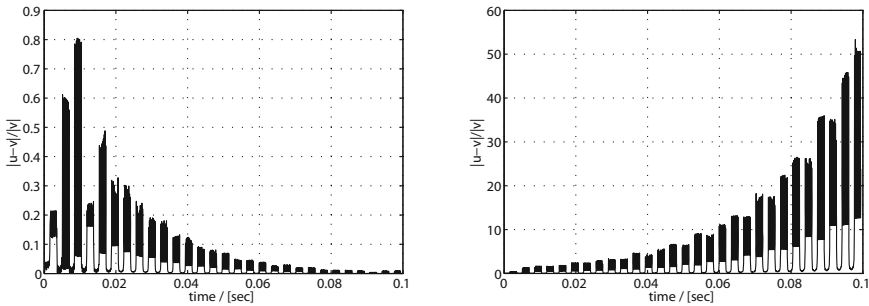


Fig. 2.9 Stable (a) and unstable (b) solutions of system (2.53)

In the stable case, the solution of (2.53) converges to the solution of the corresponding ODE. Consequently, the relative difference of both solutions converges to zero. Such an evolution of the relative difference is shown in Fig. 2.9(a). In the unstable case, the solution of (2.53) does not converge to the solution of the corresponding ODE, which remains bounded for all times. Consequently the relative difference of both solutions diverges, as illustrated by Fig. 2.9(b). In the experiments, the evolution of the DDE-solution is called chatter. While the DDE model properly reproduces the onset of chatter the ODE model has a bounded solution of all positive values of a_p and is thus not capable of reproducing chatter phenomena.

2.4.2 Simulation

In the previous sections, the different approaches of modeling of the machine and the process behavior have been presented. The coupling of the models differs for the different processes. This section gives a short overview of the simulation

techniques, which have been applied within the different projects of the priority program.

Within the Priority Program 1180, the analysis of the process machine interactions for cutting operations focuses on the coupling of process forces and the deflection of the tool. As shown in the example of a simple milling model, the coupling for cutting processes is given by a change of the intersection between tool and workpiece:

- change of cutting geometry caused by the deflection of the tool/workpiece
- modulation of cutting forces caused by the changing cutting geometry

For the computation of the tool workpiece intersection the following approaches have been applied:

- intersection between a discrete workpiece (e. g. Dixel model) and the envelope of the tool (e. g. CSG model)
- intersection between a discrete workpiece and a micro-model of single grains as well as a macro-model of the grinding wheel for abrasive processes
- analytical computation of the chip thickness, as shown in the example in the preceding section

In sheet metal forming, the position and deformation of the tool represent the boundary conditions for the FE simulations of the forming of the blank. The resulting forces at the nodes of the blank model act on the tool causing deflections and deformations. For the computation of static or dynamic interaction respectively two principle methods have been applied.

- Offline coupling, i. e. iterative computation of process forces and deflections of the ram
- Integration of the model of the machine in the FE model of the forming process

For the simulation of commercial software tools as well as in-house developments were used. The coupling was carried out in the same solver or by coupled simulations.

- Exchange of forces and deflections between two simulators with a fixed time step
- Exchange of forces and deflections between two simulators with a variable time step
- Exchange of forces and deflections in the same tool (model integration, time domain simulations)
- Mode-dependent exchange of forces and deflections in the same tool.
- Integration of a force model in the equations of motion. Taking the repetitive tooth engagement into account leads to a system of delayed differential equations.

The different simulation techniques are illustrated in Fig. 2.10

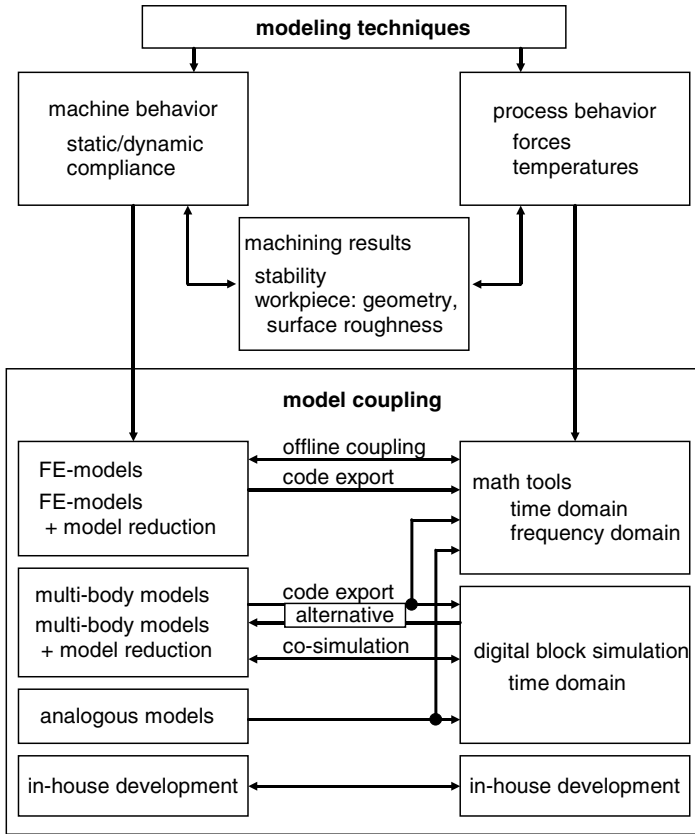


Fig. 2.10 Simulation techniques applied in the Priority Program 1180

2.5 Conclusion

An overview of the applied modeling approaches has been provided. It has been demonstrated which approach is suitable under specific conditions regarding the machine and process behavior. An overview of the coupling methods and the simulation techniques has also been given. The choice as to which approach has to be applied depends on the intension of the simulation of the process machine interaction, i. e. the interaction phenomenon that is to be investigated. This chapter has given only basic information on the principle methods. Detailed information will be provided in the following chapters, showing the application of these approaches to the project specific problems.

References

- [1] Brecher, C., Esser, M., Witt, S.: Interaction of manufacturing process and machine tool. *CIRP Annals – Manufacturing Technology* 58, 588–607 (2009)
- [2] Klocke, F., Brecher, C., Sitte, B., Weiß, M.: Analyse der dynamischen Wechselwirkungen bei Pendel- und Schnellhubschleifprozessen. In: *Jahrbuch Schleifen, Honen, Läppen und Polieren*, vol. 64, Ausgabe, Essen (2010)
- [3] Hoffmann, F.: Optimierung der dynamischen Bahngenaugigkeit von Werkzeugmaschinen mit der Mehrkörpersimulation. Dissertation, WZL of RWTH Aachen University (2008)
- [4] Oden, J.T., Lin, T.L.: On the general rolling contact problem for finite deformations of a viscoelastic cylinder. *Computer Methods in Applied Mechanics and Engineering* 57, 297–367 (1986)
- [5] Thusty, J.: Analysis of the State of Research in Cutting Dynamics. *Annals of the CIRP* 27(2), 583–589 (1978)
- [6] Radharamanan, R.: The Measurement of the Dynamic Cutting Coefficients and the Analysis of Chatter Behaviour in Turning. Katholieke Universiteit Leuven, Dissertation (1977)
- [7] Altintas, Y., Weck, M.: Chatter Stability of Metal Cutting and Grinding. In: *Annals of the CIRP*, vol. 53(2), pp. 619–642 (2004)
- [8] Stephenson, D.A., Agapiou, J.S.: *Metal Cutting. Theory and Practice*. Marcel Dekker Inc., New York (1996)
- [9] Merchant, M.E.: Mechanics of the metal cutting process. *Journal of Applied Physics* 16, 318–325 (1945)
- [10] Fang, N., Jaehir, I.S.: Analytical Predictions and Experimental Validation of Cutting Forces Ratio, Chip Thickness, and Chip Back-Flow Angle in Restricted Contact Machining Using the Universal Slip-Line Model. *International Journal of Machine Tools and Manufacture* 42, 681–694 (2000)
- [11] Clausen, M.: Zerspankraftprognose und -simulation für Dreh- und Fräsprozesse. Hannover. Diss (2005)
- [12] Thusty, J., Ismail, F.: Basic Non-Linearity in Machining Chatter. *Annals of the CIRP* 30(1), 299–304 (1981)
- [13] Altintas, Y.: Modeling Approaches and Software for Predicting the Performance of Milling Operations at MAL-UBC. *Machining Science and Technology* 4(4), 445–478 (2000)
- [14] Weck, M., Brecher, C.: *Werkzeugmaschinen. Automatisierung von Maschinen und Anlagen*; 6. Auflage. Springer (2006)
- [15] Stépán, G., Insperger, T.: Stability of the Milling Process. *Periodica Polytechnica Ser. Mech. Eng.* 44 (2000)
- [16] Feng, H.-Y., Azeem, A., Wang, L.: Simplified and Efficient Calibration of a Mechanistic Cutting Force Model for Ball-End Milling. *International Journal of Machine Tools and Manufacture* 44, 214–268 (2004)
- [17] Witt, S.: Integrierte Simulation von Maschine, Werkstück und spanendem Fertigungsprozess. Dissertation. Aachen. RWTH Aachen, Werkzeugmaschinenlabor RWTH Aachen (2007)
- [18] Marsolek, J., Fleischer, J., Schmidt, C., Schermann, T.: Simulation von Zerspanungsprozessen mit Abaqus. Tagungsband ABAQUS Benutzerkonferenz, Nürnberg (2005)

- [19] Kim, J.S., Lee, B.H.: An Analytical Model of Dynamic Cutting Forces in Chatter Vibration. *International Journal of Machine Tools and Manufacture* 31(3), 371–381 (1991)
- [20] van Brussel, H.: Dynamische Analyse van het Verspaningsproces. Katholieke Universiteit Leuven, Dissertation (1971)
- [21] Werntze, G.: Dynamische Schnittkraftkoeffizienten. Bestimmung mit Hilfe des Digitalrechners und Berücksichtigung im mathematischen Modell zur Stabilitätsanalyse. RWTH Aachen, Dissertation (1973)
- [22] Brinksmeier, E., Aurich, J.C., Govekar, E., Heinzl, C., Hoffmeister, H.W., Peters, J., Rentsch, R., Stephenson, D.J., Uhlmann, E., Weinert, K., Wittmann, M.: Advances in Modeling and Simulation of Grinding Processes. *Annals of the CIRP* 55(2), 667–696 (2006)
- [23] Tönshoff, H.K., Peters, J., Inasaki, T., Paul, T.: Modelling and Simulation of Grinding Processes. *Annals of the CIRP* 41(2), 677–688 (1992)
- [24] Aurich, J.C., Biermann, D., Blum, H., Brecher, C., Carstensen, C., Denkena, B., Klocke, F., Kröger, M., Steinmann, P., Weinert, K.: Modelling and simulation of process: machine interaction in grinding. *Production Engineering* 3(1), 111–120
- [25] Mackerle, J.: Finite Element Analysis and Simulation of Machining: an Addendum. A Bibliography (1996-2002). *International Journal of Machine Tools & Manufacture* 43, 103–114 (2003)
- [26] Hou, Z.B., Komanduri, R.: On the Mechanics of the Grinding Process-Part 1. Stochastic Nature of the Grinding Process. *International Journal of Machine Tools & Manufacture* 43, 1579–1593 (2003)
- [27] Zitt, U.-R.: Modellierung und Simulation von Hochleistungsschleifprozessen. University of Kaiserslautern, Dissertation (1999)
- [28] Chang, H.-C., Junz Wang, J.-J.: A stochastic grinding force model considering random grit distribution. *International Journal of Machine Tools and Manufacture* 48, 1335–1344 (2008)
- [29] Doman, D.A., Warkentin, A., Bauer, R.: Finite element modeling approaches in grinding. *International Journal of Machine Tools and Manufacture* 49(2), 109–116
- [30] Werner, K., Klocke, F., Brinksmeier, E.: Modelling and Simulation of Grinding Processes. In: 1st European Conference on Grinding. Aachen, pp. S.8-1 – S.8-27 (2003)
- [31] Denkena, B., Deichmueller, M., Kröger, M., Popp, K.M., Carstensen, C., Schroeder, A., Wiedemann, S.: Geometrical Analysis of the Complex Contact Area for Modeling the local Distribution of Process Forces in Tool Grinding. In: Proceedings of the 1st International Conference on Process Machine Interaction, pp. 289–298 (2008)
- [32] Voelkner, W.: Spannungs- Kraft- und Arbeitermittlung beim Umformen. *Fertigungstechnik und Betrieb* 25(12), 739–743 (1975)
- [33] Voelkner, W.: Ein Beitrag zur Streifen- und Gleitlinienmethode. *Wissenschaftliche Zeitschrift der TU Dresden* 25(3), 613–618 (1976)
- [34] Lange, K. (ed.): Handbook of Metal Forming. Society of Manufacturing Engineers, Dearborn, MI (1994)
- [35] Petzold, W., König, J., Eberlein, L. (eds.): Umform- und Zerteiltechnik. Lehrbrief Tiefziehen und Drücken, Dresden (1981)
- [36] Neugebauer, R. (ed.): Umform- und Zerteiltechnik. Verlag Wissenschaftliche Skripten, Chemnitz (2005)